A&A 525, A44 (2011)
DOI: 10.1051/0004-6361/201015006

Astronomy & Astrophysics

Infrared Mn I laboratory oscillator strengths for the study of late type stars and ultracool dwarfs

R. Blackwell-Whitehead[1,2], Y. V. Pavlenko[3,4], G. Nave[5], J. C. Pickering[2], H. R. A. Jones[3], Y. Lyubchik[4], and H. Nilsson[1]

[1] Lund Observatory, Box 43, 221 00 Lund, Sweden
e-mail: r.blackwell@astro.lu.se
[2] Blackett Laboratory, Imperial College London, London SW7 2AZ, UK
[3] Centre for Astrophysics Research, University of Hertfordshire, College Lane, Hatfield, Hertfordshire AL10 9AB, UK
[4] Main Astronomical Observatory of the Academy of Sciences of Ukraine, Zabolotnoho 27, Kyiv 03680, Ukraine
[5] Atomic Physics Division, National Institute of Standards and Technology, 100 Bureau Dr., Gaithersburg, MD 20899, USA

Received 17 May 2010 / Accepted 3 September 2010

ABSTRACT

Aims. The aim of our new laboratory measurements is to measure accurate absolute oscillator strengths for neutral manganese transitions in the infrared needed for the study of late-type stars and ultracool dwarfs.

Methods. Branching fractions have been measured by high resolution Fourier transform spectroscopy and combined with radiative level lifetimes in the literature to yield oscillator strengths.

Results. We present experimental oscillator strengths for 20 Mn I transitions in the wavelength range 3216 to 13 997 Å, 15 of which are in the infrared. The transitions at 12 899 Å and 12 975 Å are observed as strong features in the spectra of late-type stars and ultracool dwarfs. We have fitted our calculated spectra to the observed Mn I lines in spectra of late-type stars. Using the new experimentally measured Mn I $\log(gf)$ values together with existing data for Mn I hyperfine structure splitting factors we determined the manganese abundance to be $\log N(\mathrm{Mn}) = -6.65 \pm 0.05$ in the atmosphere of the Sun, $\log N(\mathrm{Mn}) = 6.95 \pm 0.20$ in the atmosphere of Arcturus, and $\log N(\mathrm{Mn}) = -6.70 \pm 0.20$ in the atmosphere of M 9.5 dwarf 2MASSW 0140026+270150.

Key words. atomic data – line: identification – methods: laboratory – stars: late-type

1. Introduction

Manganese is an iron-peak element and the nucleosynthesis path that leads to its formation is relatively well understood. However, it remains unclear which objects are the main donors of manganese to the Galaxy at different times of its evolution. Nevertheless, manganese is widely used for the investigation of the chemical evolution of the disk and halo of our Galaxy (see Sobeck et al. 2006, and references therein).

Accurate atomic oscillator strengths (f-values and $\log(gf)$) are required for the correct interpretation of the physical properties and processes in stellar and sub-stellar objects. In particular, oscillator strengths for atomic lines in the infrared (IR) spectral region are needed for the study of the spectra of late-type stars, ultracool dwarfs, and dust obscured objects such as young stars and the centre of galaxies. Accurate oscillator strengths are of particular importance to the study of late type stars and ultracool dwarfs where the spectral energy distribution peaks in the IR and is dominated by spectral lines from neutral atoms and molecules (see Lyubchik et al. 2004; Jones et al. 2005).

Over the past ten years there has been an increase in IR spectral observations of astrophysical objects with the advent of new IR spectrographs on ground based and satellite borne telescopes. However, there are only a relatively small number of experimentally measured oscillator strengths for IR spectral lines compared to the number of measured oscillator strengths for visible spectral lines available in the literature. The status of oscillator strengths in the atomic database has been discussed by Wahlgren & Johansson (2003), Johansson (2005), Brickhouse et al. (2006) and Blackwell-Whitehead et al. (2008), and there have been calls for more IR measurements including Lyubchik et al. (2004), and Bigot & Thévenin (2006).

The current laboratory atomic database for Mn I oscillator strengths is dominated by transitions in the UV and visible. Our previous oscillator strength measurements for Mn I, Blackwell-Whitehead et al. (2005a), include 44 transitions from 2090 to 27 800 Å of which six transitions are in the IR. Only eleven experimentally measured oscillator strengths for Mn I have been published for $\lambda > 6520$ Å, see Blackwell-Whitehead et al. (2005a). Booth et al. (1984) reported 58 Mn I f-values including the UV and visible resonance transitions from the $3d^5(^6S)4s4p\ z\ ^4P^\circ_J$ and $3d^5(^6S)4s4p\ z\ ^6P^\circ_J$ levels. However, no f-values have been published for the IR transitions from the $z\ ^4P^\circ_J$ and $z\ ^6P^\circ_J$ levels despite these transitions being amongst the strongest Mn I transitions for $10\,000 < \lambda < 15\,000$ Å. In our current work we measured Mn I oscillator strengths for transitions from the $z\ ^4P^\circ_J$ and $z\ ^6P^\circ_J$ upper levels by combining branching fractions (BFs) measured by high resolution Fourier transform spectrometry with known level lifetimes (τ). These include the 12 899 Å and 12 875 Å spectral lines that are observed as strong features in the spectra of ultracool dwarf stars, see Lyubchik et al. (2007).

2. Laboratory measurements

The oscillator strengths have been determined by combining BFs with radiative lifetimes in the same manner as described

in Blackwell-Whitehead et al. (2005a). The spectrum of Mn I was recorded in the UV to visible spectral range (1600 Å to 8000 Å) using the Imperial College high resolution Fourier transform spectrometer (FTS) (Pickering 2002), and in the visible to IR spectral range (3500 Å to 55 000 Å) using the 2m FTS at the National Institute of Standards and Technology (NIST) (Nave et al. 1997). The light source for the NIST and Imperial College measurements was a hollow cathode lamp (HCL) with a manganese cathode using either an argon or neon buffer gas. Two manganese cathodes were used in these measurements. The NIST cathode was an alloy of 95% manganese and 5% copper, the cathode used at Imperial College was an alloy of 88% manganese and 12% nickel. The optimal running conditions for the HCL were found to be a pressure of 340 Pa of neon with currents of 200 mA to 500 mA. Further details of the measurements and their analysis are given in Blackwell-Whitehead et al. (2005a). The spectra were recorded at a range of currents to determine an intensity versus current curve of growth for each line to determine if any lines were self absorbed, which would lead to erroneous relative line intensities. It was found that a HCL current of 200 mA was used to observe absorption free spectra of the UV and visible resonance lines and a higher HCL current of 500 mA was used for the measurement of the relatively weaker IR transitions. In addition, the line profile of each transition was fitted using published hyperfine structure (HFS) constants for the upper and lower level of the transition (Handrich et al. 1969; Dembczyński et al. 1979; Brodzinski et al. 1987; Blackwell-Whitehead et al. 2005b). The residual value of the fit was found to be the same as the background noise level indicating that no self absorption was present.

The manganese spectra were intensity calibrated using tungsten intensity standard lamps. The Imperial College tungsten intensity standard lamp was calibrated by the National Physical Laboratory, UK, and the NIST tungsten intensity standard lamp was calibrated by Optronics Laboratories[1]. Both lamps have a minimum radiance uncertainty of 3 percent in the spectral region used for the intensity calibration. The tungsten spectra were recorded before and after the manganese spectra and compared to determine if the instrumental response had changed during measurement of the manganese spectrum. In each case, the instrument response did not vary by more than the uncertainty in the relative radiance of the tungsten lamp. The measured tungsten spectra were used to determine the instrument response, and this was used to calibrate the relative intensity of the Mn I lines. The Mn I line profiles were fitted by employing a centre of gravity fit using the XGremlin software by Nave et al. (1997). To observe all lines from the $z\ ^4\mathrm{P}^\circ_J$ and $z\ ^6\mathrm{P}^\circ_J$ upper levels, spectra were recorded in two overlapping spectral regions. The intensity calibration of the visible to IR region was placed on the same intensity scale as the UV to visible region using intermediate transitions in the 18 000 cm^{-1} to 18 500 cm^{-1} region ($3d^6(^5D)4s\ a\ ^6D_J$–$3d^5(^6S)4s4p\ y\ ^6P^\circ_J$). The intermediate transitions are from upper levels with the same configuration and comparable level energy, which indicates that the $z\ ^4\mathrm{P}^\circ_J$, $z\ ^6\mathrm{P}^\circ_J$ and $y\ ^6\mathrm{P}^\circ_J$ levels have comparable level populations. Curves of growth for the intermediate lines indicated that no self absorption was present. Furthermore, an estimate of the change in level population between the $z\ ^4\mathrm{P}^\circ_J$, $z\ ^6\mathrm{P}^\circ_J$ and $y\ ^6\mathrm{P}^\circ_J$ levels was measured by comparing the intensity ratios between the a $^6\mathrm{D}_J$–$y\ ^6\mathrm{P}^\circ_J$ transitions and transitions from the $z\ ^4\mathrm{P}^\circ_J$ and $z\ ^6\mathrm{P}^\circ_J$ upper levels under different HCL conditions. The intensity ratios did not vary by more than the uncertainty in the measured relative line intensities, indicating that the level populations remained constant to within a few percent.

[1] Certain trade names and products are mentioned in the text in order to adequately identify the apparatus used to obtain the measurements. In no case does such identification imply recommendation or endorsement by NIST or any of the coauthor institutes.

3. Laboratory oscillator strengths

Table 1 presents the *BF*s, transition probabilities and oscillator strengths. The oscillator strengths were obtained by combining the *BF*s with the published radiative lifetimes of Kronfeldt et al. (1985) and Schnabel et al. (1995). The Mn I Ritz wavenumbers in Table 1 are determined from the upper and lower energy level values from the NIST atomic Spectra Database (Ralchenko et al. 2009), which are taken from the term analysis of Catalán et al. (1964). The air wavelengths in Table 1 have been determined with the Edlén (1966) equation, and include the more recent update for the refractive index of air, Eq. (3) in Birch & Downs (1994). All lines measured in this work have a peak signal to noise ratio of more than 100, and the *BF* uncertainties are dominated by the tungsten lamp calibration uncertainty and the uncertainty in the intensity calibration "cross-over" between the two spectral regions. The uncertainty in the oscillator strength is determined from the *BF* and lifetime uncertainty using the criteria discussed by Sikström et al. (2002) and follows the NIST guidelines for evaluating and expressing uncertainty (Taylor & Kuyatt 1994).

It can be seen that our oscillator strengths for the transitions from the $z\ ^6\mathrm{P}^\circ_J$ levels agree, to within the uncertainty, with the previous UV and visible measurements by Booth et al. (1984). There is also a good agreement with our laboratory $\log(gf)$ values for the transitions from the $z\ ^6\mathrm{P}^\circ_J$ levels and the semi-empirical calculated $\log(gf)$ values of Kurucz & Bell (1995). The measured $\log(gf)$ values for UV transitions from the $z\ ^4\mathrm{P}^\circ_J$ levels agree with both Booth et al. (1984) and Kurucz & Bell (1995) to within the uncertainties. However, the semi-empirical $\log(gf)$ values of Kurucz & Bell (1995) for IR transitions from the $z\ ^4\mathrm{P}^\circ_J$ levels are approximately 30% (0.12 dex where the unit dex is $\log_{10}$ of the ratio of the two values) stronger than our values. The difference between the measured $\log(gf)$s and the semi-empirical $\log(gf)$s is larger than the uncertainty in the measured values. It is possible that the semi-empirical calculations predict more level mixing than is present in the actual system. If the $z\ ^4\mathrm{P}^\circ_J$ levels have less mixing than predicted by the semi-empirical calculations of Kurucz & Bell (1995), then the measured $\log(gf)$s will be weaker.

The effect of hyperfine splitting on the fine structure levels and on the line profiles of Mn I transitions in the IR can be seen in an example shown in Fig. 1. The hyperfine splitting increases the width and decreases the peak intensity of the line profile. Prochaska & McWilliam (2000) discuss the importance of including hyperfine splitting in the analysis of elemental abundances in stars. In particular, if HFS is not taken into account, the chemical elemental abundance may be underestimated or it may erroneously be assumed that the line is blended with some unknown feature. To assist in the correct interpretation of the oscillator strengths in Table 1 we provide wavenumbers, wavelengths and oscillator strengths in Table 2 for the HFS component lines in the IR transitions $3d^6(^5D)4s\ a\ ^6D_J$–$3d^5(^6S)4s4p\ z\ ^6P^\circ_J$ and $3d^6(^5D)4s\ a\ ^4D_J$–$3d^5(^6S)4s4p\ z\ ^4P^\circ_J$.

The wavenumber of each transition from the upper hyperfine structure level to the lower hyperfine structure level, $\sigma_{\mathrm{HFS\ trans}}$,

Table 1. New and remeasured laboratory oscillator strengths for Mn I.

Upper level	Lower level[a]	Wavenumber[b] (cm^{-1})	λ_{air} (Å)	*BF*	*BF Unc.* (%)	*TP*[c] (10^7 s^{-1})	This Work log(*gf*)	This Work Unc. (dex)[d]	Previous Work[e] log(*gf*)	Previous Work[e] Unc. (dex)	Calc.[f] log(*gf*)
$3d^5(^6S)4s4p\ z\ ^6P^\circ_{7/2}$	a $^6S_{5/2}$	24 802.25	4030.75	0.965	4	16.01 (0.80)	−0.51	0.02	−0.47	0.08	−0.52
E = 24 802.25 cm^{-1}	a $^6D_{9/2}$	7749.96	12 899.76	0.026	13	0.43 (0.05)	−1.07	0.05			−1.06
τ = 60.3 ± 1.3 ns[g]	a $^6D_{7/2}$	7520.25	13 293.80	0.007	13	0.12 (0.02)	−1.58	0.05			−1.61
	a $^6D_{5/2}$	7350.73	13 600.37	0.001	13	0.02 (0.003)	−2.33	0.05			−2.40
Residual				0.000							
$3d^5(^6S)4s4p\ z\ ^6P^\circ_{5/2}$	a $^6S_{5/2}$	24 788.05	4033.06	0.967	4	15.16 (0.76)	−0.65	0.02	−0.62	0.08	−0.62
E = 24 788.05 cm^{-1}	a $^6D_{7/2}$	7506.05	13 318.94	0.017	13	0.27 (0.03)	−1.37	0.05			−1.36
τ = 63.8 ± 1.4 ns[f]	a $^6D_{5/2}$	7336.53	13 626.96	0.012	13	0.19 (0.02)	−1.51	0.05			−1.52
	a $^6D_{3/2}$	7219.57	13 847.46	0.004	13	0.06 (0.01)	−1.98	0.05			−2.00
Residual				0.000							
$3d^5(^6S)4s4p\ z\ ^6P^\circ_{3/2}$	a $^6S_{5/2}$	24 779.32	4034.48	0.969	4	14.66 (0.73)	−0.84	0.02	−0.81	0.08	−0.81
E = 24 779.32 cm^{-1}	a $^6D_{5/2}$	7327.80	13 642.93	0.009	13	0.14 (0.02)	−1.82	0.05			−1.81
τ = 66.1 ± 1.4 ns[f]	a $^6D_{3/2}$	7210.84	13 864.22	0.013	13	0.20 (0.03)	−1.65	0.05			−1.64
	a $^6D_{1/2}$	7142.11	13 997.52	0.009	13	0.14 (0.02)	−1.78	0.05			−1.79
Residual				0.000							
$3d^5(^6S)4s4p\ z\ ^4P^\circ_{5/2}$	a $^6S_{5/2}$	31 001.15	3224.76	0.348	8	0.36 (0.04)	−2.47	0.04	−2.45	0.08	−2.48
E = 31 001.15 cm^{-1}	a $^4D_{7/2}$	7704.48	12 975.91	0.524	6	0.54 (0.04)	−1.09	0.03			−0.94
τ = 970 ± 50 ns[f]	a $^4D_{5/2}$	7451.95	13 415.64	0.113	9	0.12 (0.01)	−1.73	0.04			−1.60
	a $^4D_{3/2}$	7281.63	13 729.44	0.013	10	0.01 (0.001)	−2.65	0.04			−2.57
Residual				0.002							
$3d^5(^6S)4s4p\ z\ ^4P^\circ_{3/2}$	a $^6S_{5/2}$	31 076.42	3216.95	0.261	8	0.23 (0.02)	−2.84	0.04	−2.82	0.08	−2.82
E = 31 076.42 cm^{-1}	a $^4D_{5/2}$	7527.22	13 281.49	0.473	6	0.42 (0.03)	−1.35	0.03			−1.23
τ = 1120 ± 50 ns[f]	a $^4D_{3/2}$	7356.90	13 588.97	0.229	8	0.21 (0.02)	−1.64	0.04			−1.53
	a $^4D_{1/2}$	7257.55	13 774.99	0.035	9	0.03 (0.003)	−2.45	0.04			−2.35
Residual				0.002							

Notes. [(a)] Full term designations for the lower levels are $3d^6(^5D)4s\ a^{4,6}D_J$ and $3d^5(^6S)4s^2\ a^6S_{5/2}$. [(b)] Ritz wavenumber. [(c)] Transition probability, the uncertainty is given in brackets (±). [(d)] The uncertainty in the log(*gf*) is expressed in dex, where ±0.01 dex corresponds to approximately ±2.5 per cent. [(e)] The previous laboratory log(*gf*)s from Booth et al. (1984), the uncertainties in the log(*gf*)s of Booth et al. (1984) are those assigned by NIST, Fuhr & Wiese (2003). [(f)] Semi-empirical log(*gf*) calculations of Kurucz & Bell (1995). [(g)] Radiative lifetime values, τ, for $z\ ^6P^\circ_J$ are from Schnabel et al. (1995) and for $z\ ^4P^\circ_J$ are from Kronfeldt et al. (1985).

in Table 2 is determined from the wavenumber for the fine-structure transition, σ_{FS}, using:

$$\sigma_{HFS\ trans} = \sigma_{FS} - \frac{K_l A_l}{2} + \frac{K_u A_u}{2} \quad (1)$$

where A_u and A_l are the magnetic dipole hyperfine interaction constants for the upper and lower fine structure levels; and K is defined as:

$$K = F(F+1) - J(J+1) - I(I+1) \quad (2)$$

where F is the quantum number associated with the total angular momentum of the electrons, J, and the nuclear spin, I. For manganese the spin of the nucleus $I = 5/2$. Equation (1) excludes the contribution from the electric quadrupole hyperfine interaction constant B which is relatively small when compared to the magnetic dipole hyperfine interaction constant A for the levels considered in this paper, see Kuhn (1964).

Several of the IR transitions included in our work (12 899.8, 12 975.9, 13 281.5, 13 319.0, and 13 642.9 Å) have been studied by Meléndez (1999) who has determined the wavelength of individual hyperfine structure components by analysing Mn I transitions in solar photospheric spectra. However, Meléndez notes that several of these lines have blended features and he does not provide HFS constants for the upper and lower levels of the transitions.

4. Modelling Mn I lines in the spectra of the Sun, Arcturus and ultracool dwarfs

We have computed the synthetic spectra of late-type stars and brown dwarfs using the WITA6 programme (Pavlenko 2000). The model atmospheres for the Sun (spectral classification = G2V, T_{eff}/ log(g) = 5770/4.44, and abundances from Gurtovenko & Kostik 1989), and Arcturus (K2III, 4300/1.5, and abundances from Peterson et al. 1993) have been computed with ATLAS12 (Kurucz 1993; Pavlenko 2003). The calculated spectra of the brown dwarf 2MASSW 0140026+270150 were computed with the DUSTY 2000/4.5/0 model atmosphere (Allard et al. 2001). The atomic line data for species other than Mn I were taken from the Vienna Atomic Line Database (VALD) (Kupka et al. 1999). We used molecular line lists from different sources: TiO (Plez 1998), FeH (Dulick et al. 2003), CrH (Burrows et al. 2002) as well as H_2O line list BT2 (Barber et al. 2006). For Arcturus we used the abundances of Peterson et al. (1993) and the spectra of the Sun and brown dwarfs were computed with the solar abundances reported by Anders & Grevesse (1989). The absorption lines are hyperfine split and each hyperfine component line (Table 2) has been fitted using the Voigt function $H(a, v)$ and the formulae of Unsöld (1955) to calculate the damping constants. Theoretical spectra were computed with a wavelength step 0.01Å and convolved with Gaussians to match

Table 2. Wavenumber and wavelength of the HFS component lines in the IR transitions $3d^6(^5D)4s$ a $^6D_J - 3d^5(^6S)4s4p$ z $^6P^\circ_J$ and $3d^6(^5D)4s$ a $^4D_J - 3d^5(^6S)4s4p$ z $^4P^\circ_J$.

Upper level	Lower level	HFS Constants (cm^{-1})[a]				HFS levels		HFS transitions[b]		HFS Comp.[c]
		A_{upper}	B_{upper}	A_{lower}	B_{lower}	F_{upper}	F_{lower}	$\sigma(cm^{-1})$	λ_{air}(Å)	$\log(gf)$
z $^6P^\circ_{7/2}$	a $^6D_{9/2}$	0.0143	0.0022	0.0170	0.0044	6.0	5.0	7750.1163	12 899.5037	−4.18
		(0.0001)	(0.0001)	(0.0003)	(0.0040)	5.0	4.0	7750.1143	12 899.5071	−3.85
						4.0	3.0	7750.1099	12 899.5144	−3.75
						3.0	2.0	7750.1031	12 899.5256	−3.88
						2.0	2.0	7750.0607	12 899.5962	−2.78
						3.0	3.0	7750.0530	12 899.6090	−2.60
						4.0	4.0	7750.0427	12 899.6262	−2.54
						1.0	2.0	7750.0325	12 899.6431	−2.27
						5.0	5.0	7750.0297	12 899.6478	−2.58
						6.0	6.0	7750.0141	12 899.6738	−2.77
						2.0	3.0	7750.0106	12 899.6797	−2.14
						3.0	4.0	7749.9858	12 899.7208	−2.01
						4.0	5.0	7749.9582	12 899.7669	−1.89
						5.0	6.0	7749.9275	12 899.8179	−1.78
						6.0	7.0	7749.8937	12 899.8742	−1.67
z $^4P^\circ_{5/2}$	a $^4D_{7/2}$	−0.0203	0.0025	−0.0054	0.0000	0.0	1.0	7704.5977	12 975.7138	−2.65
		(0.0001)	(0.0005)	(0.0001)	(−)	1.0	2.0	7704.5878	12 975.7305	−2.36
						1.0	1.0	7704.5770	12 975.7487	−2.62
						2.0	3.0	7704.5628	12 975.7727	−2.14
						2.0	2.0	7704.5466	12 975.7999	−2.44
						2.0	1.0	7704.5358	12 975.8181	−3.39
						3.0	4.0	7704.5229	12 975.8399	−1.96
						3.0	3.0	7704.5013	12 975.8762	−2.37
						3.0	2.0	7704.4851	12 975.9035	−3.32
						4.0	5.0	7704.4686	12 975.9313	−1.80
						4.0	4.0	7704.4416	12 975.9768	−2.40
						4.0	3.0	7704.4200	12 976.0132	−3.44
						5.0	6.0	7704.4005	12 976.0460	−1.66
						5.0	5.0	7704.3681	12 976.1006	−2.57
						5.0	4.0	7704.3411	12 976.1460	−3.79
z $^4P^\circ_{3/2}$	a $^4D_{5/2}$	−0.0271	−0.0013	−0.0046	0.0000	1.0	2.0	7527.3355	13 281.2812	−2.76
		(0.0001)	(0.0010)	(0.0001)	(−)	1.0	1.0	7527.3263	13 281.2975	−2.58
						1.0	0.0	7527.3217	13 281.3056	−2.91
						2.0	3.0	7527.2957	13 281.3513	−2.35
						2.0	2.0	7527.2819	13 281.3756	−2.43
						2.0	1.0	7527.2727	13 281.3919	−2.95
						3.0	4.0	7527.2332	13 281.4616	−2.08
						3.0	3.0	7527.2148	13 281.4941	−2.41
						3.0	2.0	7527.2010	13 281.5184	−3.13
						4.0	5.0	7527.1471	13 281.6135	−1.86
						4.0	4.0	7527.1241	13 281.6541	−2.55
						4.0	3.0	7527.1057	13 281.6865	−3.51
z $^6P^\circ_{7/2}$	a $^6D_{7/2}$	0.0143	0.0022	0.0153	0.0007	6.0	5.0	7520.3334	13 293.6473	−3.18
		(0.0001)	(0.0001)	(0.0001)	(0.0013)	5.0	4.0	7520.3233	13 293.6650	−3.00
						4.0	3.0	7520.3129	13 293.6835	−2.97
						3.0	2.0	7520.3018	13 293.7031	−3.03
						2.0	1.0	7520.2898	13 293.7243	−3.23
						1.0	1.0	7520.2616	13 293.7741	−2.98
						2.0	2.0	7520.2593	13 293.7782	−2.91
						3.0	3.0	7520.2560	13 293.7840	−2.74
						4.0	4.0	7520.2518	13 293.7915	−2.54
						5.0	5.0	7520.2468	13 293.8003	−2.36
						6.0	6.0	7520.2413	13 293.8100	−2.19
						1.0	2.0	7520.2312	13 293.8280	−3.23
						2.0	3.0	7520.2136	13 293.8590	−3.03
						3.0	4.0	7520.1949	13 293.8920	−2.97
						4.0	5.0	7520.1753	13 293.9268	−3.00
						5.0	6.0	7520.1548	13 293.9630	−3.18

Table 2. continued.

Upper level	Lower level	HFS Constants (cm^{-1})[a]				HFS levels		HFS transitions[b]		HFS Comp.[c]
		A_{upper}	B_{upper}	A_{lower}	B_{lower}	F_{upper}	F_{lower}	$\sigma(cm^{-1})$	λ_{air}(Å)	log(gf)
$z\ ^6P^\circ_{5/2}$	a $^6D_{7/2}$	0.0156	−0.0026	0.0153	0.0007	5.0	4.0	7506.1820	13 318.7097	−4.07
		(0.0001)	(0.0001)	(0.0001)	(0.0013)	4.0	3.0	7506.1662	13 318.7379	−3.72
						3.0	2.0	7506.1494	13 318.7676	−3.59
						2.0	1.0	7506.1325	13 318.7977	−3.67
						5.0	5.0	7506.1055	13 318.8455	−2.85
						4.0	4.0	7506.1051	13 318.8463	−2.67
						3.0	3.0	7506.1037	13 318.8488	−2.65
						2.0	2.0	7506.1020	13 318.8517	−2.72
						1.0	1.0	7506.1006	13 318.8542	−2.90
						0.0	1.0	7506.0846	13 318.8827	−2.93
						1.0	2.0	7506.0701	13 318.9083	−2.64
						2.0	3.0	7506.0562	13 318.9329	−2.42
						3.0	4.0	7506.0426	13 318.9572	−2.24
						4.0	5.0	7506.0286	13 318.9820	−2.08
						5.0	6.0	7506.0135	13 319.0088	−1.94
$z\ ^4P^\circ_{5/2}$	a $^4D_{5/2}$	−0.0203	0.0025	−0.0046	0.0000	0.0	1.0	7452.0928	13 415.3805	−3.29
		(0.0001)	(0.0005)	(0.0001)	(−)	1.0	2.0	7452.0813	13 415.4012	−3.02
						1.0	1.0	7452.0721	13 415.4178	−4.05
						1.0	0.0	7452.0675	13 415.4261	−3.29
						2.0	3.0	7452.0539	13 415.4506	−2.92
						2.0	2.0	7452.0401	13 415.4755	−3.35
						2.0	1.0	7452.0309	13 415.4920	−3.02
						3.0	4.0	7452.0108	13 415.5282	−2.93
						3.0	3.0	7451.9924	13 415.5613	−2.91
						3.0	2.0	7451.9786	13 415.5862	−2.92
						4.0	5.0	7451.9525	13 415.6332	−3.09
						4.0	4.0	7451.9295	13 415.6746	−2.58
						4.0	3.0	7451.9111	13 415.7077	−2.93
						5.0	5.0	7451.8520	13 415.8141	−2.31
						5.0	4.0	7451.8290	13 415.8555	−3.09
$z\ ^4P^\circ_{3/2}$	a $^4D_{3/2}$	−0.0271	−0.0013	0.0017	0.0000	1.0	1.0	7357.0508	13 588.6873	−3.07
		(0.0001)	(0.0010)	(0.0002)	(−)	1.0	2.0	7357.0474	13 588.6936	−2.70
						2.0	1.0	7356.9973	13 588.7861	−2.70
						2.0	2.0	7356.9939	13 588.7924	−4.28
						2.0	3.0	7356.9888	13 588.8018	−2.57
						3.0	2.0	7356.9130	13 588.9418	−2.57
						3.0	3.0	7356.9079	13 588.9513	−2.74
						3.0	4.0	7356.9011	13 588.9638	−2.67
						4.0	3.0	7356.7988	13 589.1528	−2.67
						4.0	4.0	7356.7920	13 589.1653	−2.19
$z\ ^6P^\circ_{7/2}$	a $^6D_{5/2}$	0.0143	0.0022	0.0146	−0.0016	6.0	5.0	7350.7641	13 600.3091	−2.90
		(0.0001)	(0.0001)	(0.0001)	(0.0010)	5.0	4.0	7350.7499	13 600.3353	−3.04
						4.0	3.0	7350.7368	13 600.3595	−3.20
						3.0	2.0	7350.7241	13 600.3830	−3.38
						2.0	1.0	7350.7113	13 600.4067	−3.60
						1.0	0.0	7350.6980	13 600.4314	−3.89
						1.0	1.0	7350.6831	13 600.4589	−3.86
						2.0	2.0	7350.6817	13 600.4615	−3.68
						3.0	3.0	7350.6799	13 600.4648	−3.61
						4.0	4.0	7350.6783	13 600.4677	−3.64
						5.0	5.0	7350.6775	13 600.4692	−3.81
						1.0	2.0	7350.6535	13 600.5137	−4.63
						2.0	3.0	7350.6375	13 600.5433	−4.56
						3.0	4.0	7350.6215	13 600.5729	−4.68
						4.0	5.0	7350.6060	13 600.6016	−5.03
$z\ ^6P^\circ_{5/2}$	a $^6D_{5/2}$	0.0156	−0.0026	0.0146	−0.0016	5.0	4.0	7336.6086	13 626.5500	−2.87
		(0.0001)	(0.0001)	(0.0001)	(0.0010)	4.0	3.0	7336.5901	13 626.5843	−2.71
						3.0	2.0	7336.5718	13 626.6184	−2.70
						2.0	1.0	7336.5539	13 626.6514	−2.80
						1.0	0.0	7336.5369	13 626.6831	−3.07

Table 2. continued.

Upper level	Lower level	HFS Constants (cm^{-1})[a] A_{upper}	B_{upper}	A_{lower}	B_{lower}	HFS levels F_{upper}	F_{lower}	HFS transitions[b] $\sigma(cm^{-1})$	λ_{air}(Å)	HFS Comp.[c] log(gf)
						5.0	5.0	7336.5362	13 626.6844	−2.09
						4.0	4.0	7336.5316	13 626.6929	−2.36
						3.0	3.0	7336.5276	13 626.7004	−2.69
						2.0	2.0	7336.5243	13 626.7065	−3.13
						1.0	1.0	7336.5221	13 626.7107	−3.83
						0.0	1.0	7336.5061	13 626.7404	−3.07
						1.0	2.0	7336.4925	13 626.7657	−2.80
						2.0	3.0	7336.4801	13 626.7885	−2.70
						3.0	4.0	7336.4691	13 626.8090	−2.71
						4.0	5.0	7336.4593	13 626.8273	−2.87
$z\ ^6P^\circ_{3/2}$	a $^6D_{5/2}$	0.0191	0.0006	0.0146	−0.0016	4.0	3.0	7327.9113	13 642.7230	−3.98
		(0.0001)	(0.0002)	(0.0001)	(0.0010)	3.0	2.0	7327.8787	13 642.7836	−3.60
						4.0	4.0	7327.8528	13 642.8319	−3.02
						2.0	1.0	7327.8512	13 642.8348	−3.42
						3.0	3.0	7327.8345	13 642.8659	−2.88
						1.0	0.0	7327.8282	13 642.8777	−3.38
						2.0	2.0	7327.8216	13 642.8900	−2.90
						1.0	1.0	7327.8133	13 642.9053	−3.05
						1.0	2.0	7327.7837	13 642.9605	−3.23
						4.0	5.0	7327.7804	13 642.9666	−2.33
						2.0	3.0	7327.7774	13 642.9722	−2.82
						3.0	4.0	7327.7761	13 642.9747	−2.55
$z\ ^4P^\circ_{5/2}$	a $^4D_{3/2}$	−0.0203	0.0025	0.0017	0.0000	0.0	1.0	7281.8174	13 729.0815	−4.21
		(0.0001)	(0.0005)	(0.0002)	(−)	1.0	1.0	7281.7967	13 729.1206	−3.88
						1.0	2.0	7281.7933	13 729.1270	−4.25
						2.0	1.0	7281.7554	13 729.1983	−4.06
						2.0	2.0	7281.7520	13 729.2047	−3.72
						2.0	3.0	7281.7469	13 729.2144	−4.43
						3.0	2.0	7281.6905	13 729.3207	−3.65
						3.0	3.0	7281.6854	13 729.3303	−3.71
						3.0	4.0	7281.6786	13 729.3431	−4.81
						4.0	3.0	7281.6041	13 729.4836	−3.38
						4.0	4.0	7281.5973	13 729.4964	−3.85
						5.0	4.0	7281.4968	13 729.6859	−3.16
$z\ ^4P^\circ_{3/2}$	a $^4D_{1/2}$	−0.0271	−0.0013	0.0506	0.0000	1.0	2.0	7257.7805	13 774.5508	−3.35
		(0.0001)	(0.0010)	(0.0003)	(−)	2.0	2.0	7257.7269	13 774.6523	−3.24
						3.0	2.0	7257.6460	13 774.8059	−3.34
						2.0	3.0	7257.5751	13 774.9404	−3.78
						3.0	3.0	7257.4942	13 775.0940	−3.24
						4.0	3.0	7257.3851	13 775.3011	−2.88
$z\ ^6P^\circ_{5/2}$	a $^6D_{3/2}$	0.0156	−0.0026	0.0157	−0.0022	5.0	4.0	7219.6085	13 847.3805	−2.49
		(0.0001)	(0.0001)	(0.0002)	(0.0017)	4.0	3.0	7219.5932	13 847.4099	−2.71
						3.0	2.0	7219.5784	13 847.4382	−2.98
						2.0	1.0	7219.5636	13 847.4667	−3.39
						1.0	1.0	7219.5317	13 847.5279	−3.21
						4.0	4.0	7219.5315	13 847.5282	−3.18
						2.0	2.0	7219.5310	13 847.5292	−3.06
						3.0	3.0	7219.5307	13 847.5298	−3.04
						0.0	1.0	7219.5157	13 847.5586	−3.54
						1.0	2.0	7219.4991	13 847.5903	−3.58
						2.0	3.0	7219.4832	13 847.6208	−3.76
						3.0	4.0	7219.4690	13 847.6480	−4.14
$z\ ^6P^\circ_{3/2}$	a $^6D_{3/2}$	0.0191	0.0006	0.0157	−0.0022	4.0	3.0	7210.9541	13 863.9998	−3.81
		(0.0001)	(0.0002)	(0.0002)	(0.0017)	3.0	2.0	7210.9250	13 864.0558	−3.43
						2.0	1.0	7210.8998	13 864.1041	−3.25
						4.0	4.0	7210.8912	13 864.1208	−2.85
						1.0	0.0	7210.8780	13 864.1461	−3.21
						3.0	3.0	7210.8774	13 864.1473	−2.71
						2.0	2.0	7210.8679	13 864.1656	−2.73
						1.0	1.0	7210.8620	13 864.1770	−2.88

Table 2. continued.

Upper level	Lower level	HFS Constants (cm^{-1})[a] A_{upper}	B_{upper}	A_{lower}	B_{lower}	HFS levels F_{upper}	F_{lower}	HFS transitions[b] $\sigma(cm^{-1})$	λ_{air}(Å)	HFS Comp.[c] log(gf)
						1.0	2.0	7210.8300	13 864.2384	−3.06
						2.0	3.0	7210.8202	13 864.2572	−2.65
						3.0	4.0	7210.8145	13 864.2683	−2.38
						4.0	5.0	7210.8136	13 864.2700	−2.16
$z\ ^6P^\circ_{3/2}$	a $^6D_{1/2}$	0.0191	0.0006	0.0294	0.0000	3.0	2.0	7142.1563	13 997.5468	−2.67
		(0.0001)	(0.0002)	(0.0004)	(−)	4.0	3.0	7142.1449	13 997.5693	−2.21
						2.0	2.0	7142.0992	13 997.6588	−2.57
						3.0	3.0	7142.0681	13 997.7197	−2.57
						1.0	2.0	7142.0613	13 997.7330	−2.68
						2.0	3.0	7142.0110	13 997.8316	−3.11

Notes. [(a)] The HFS A and B constants are from the published values of Dembczyński et al. (1979) for the a ^6D_J levels, Handrich et al. (1969) for the $z\ ^6P^\circ_J$ levels, Blackwell-Whitehead et al. (2005b) for the a ^4D_J levels and Brodzinski et al. (1987) for the $z\ ^4P^\circ_J$ levels. Where the B constant is quoted as 0.0000 (–) the B constant was fixed at zero in the cited reference. The uncertainty in parentheses is taken from the aforementioned references. [(b)] The wavenumber and wavelength positions for the HFS transitions have been determined from energy levels reported in the NIST atomic Spectra Database (Ralchenko et al. 2009). The relative uncertainty in the wavenumber and wavelength of the HFS transitions is determined from the uncertainty in the HFS constants for the upper and lower fine structure levels, $d\sigma_{max} = 0.001\ cm^{-1}$ and $d\lambda_{max} = 0.002$ Å. However, the wavenumber and wavelength in the table are given to four decimal places to adequately identify the hyperfine component lines. [(c)] The log(gf) for the HFS component lines is determined from the hyperfine splitting constants and log(gf) for the complete fine structure transition profile.

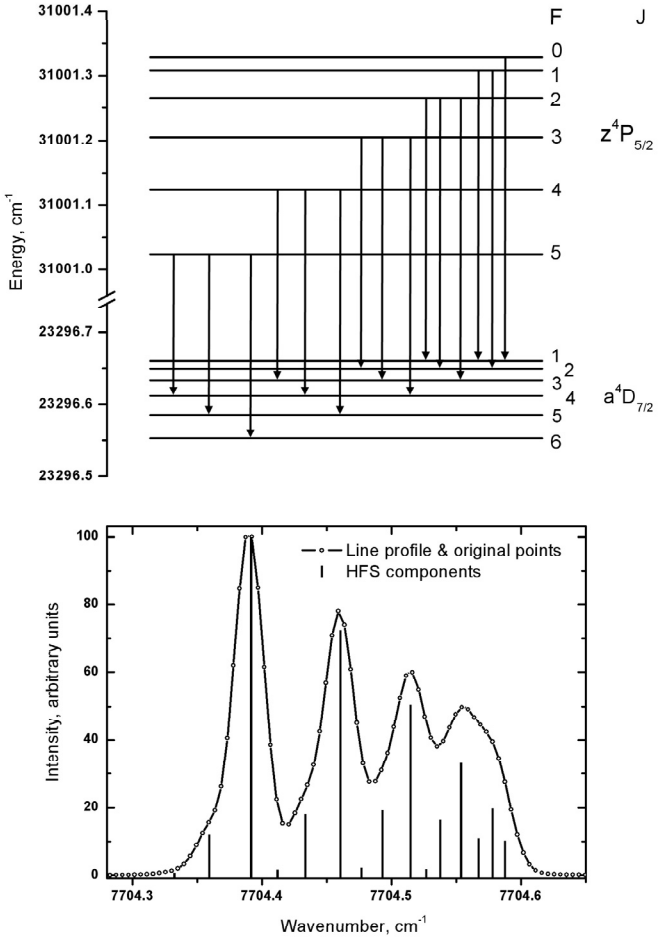

Fig. 1. The *upper plot* shows the hyperfine splitting of the fine structure levels $3d^6(^5D)4s\ a\ ^4D_{7/2}$–$3d^5(^6S)4s4p(^3P)\ z\ ^4P^\circ_{5/2}$ with allowed hyperfine transitions. The *lower plot* shows the hyperfine split profile of the transition observed in the uncalibrated laboratory spectrum at 12 975 Å, together with an indication of the positions and relative line strengths of the individual HFS transitions. A complete list of the Ritz wavelength and log(gf) for each HFS transition is available in Table 2.

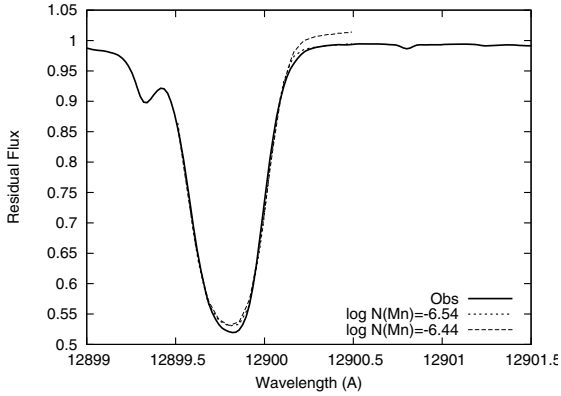

Fig. 2. The best fit to the observed solar spectrum feature found from the minima of Eq. (3) for the Mn I line at 12 899 Å.

the instrumental broadening. For Arcturus, a rotational broadening was added corresponding to a projected equatorial radial velocity $v \sin i = 7\ km\ s^{-1}$, where v is the equatorial velocity and i is the inclination of the stellar rotation axis to the line of sight to the Earth, by following the Gray (1976) formulae.

We have fitted our synthetic spectra to the observed spectra of the Sun and Arcturus atlases by Kurucz (1991) and Hinkle et al. (1995) respectively. To obtain the best fit to the observed spectra we followed the minimisation procedure described by Pavlenko & Jones (2002) and Jones et al. (2002). In summary, we find the minima of the 3D function

$$S\left(f_s, f_h, f_g\right) = \sum_\nu \left(F_\nu - F^x_\nu\right)^2, \qquad (3)$$

where F_ν and F^x_ν are the observed and computed spectra respectively, and f_s, f_h, f_g are the wavelength shift, the normalisation factor, and the profile broadening parameter, respectively. To estimate the uncertainty of the best fit we use the parameter $\Delta S = \sqrt{\frac{S}{N(N-1)}}$, where N is the number of points in the observed spectrum. We provide an example of the profile fit for the Mn I at 12 899 Å line in the spectrum of the Sun in Fig. 2 and the

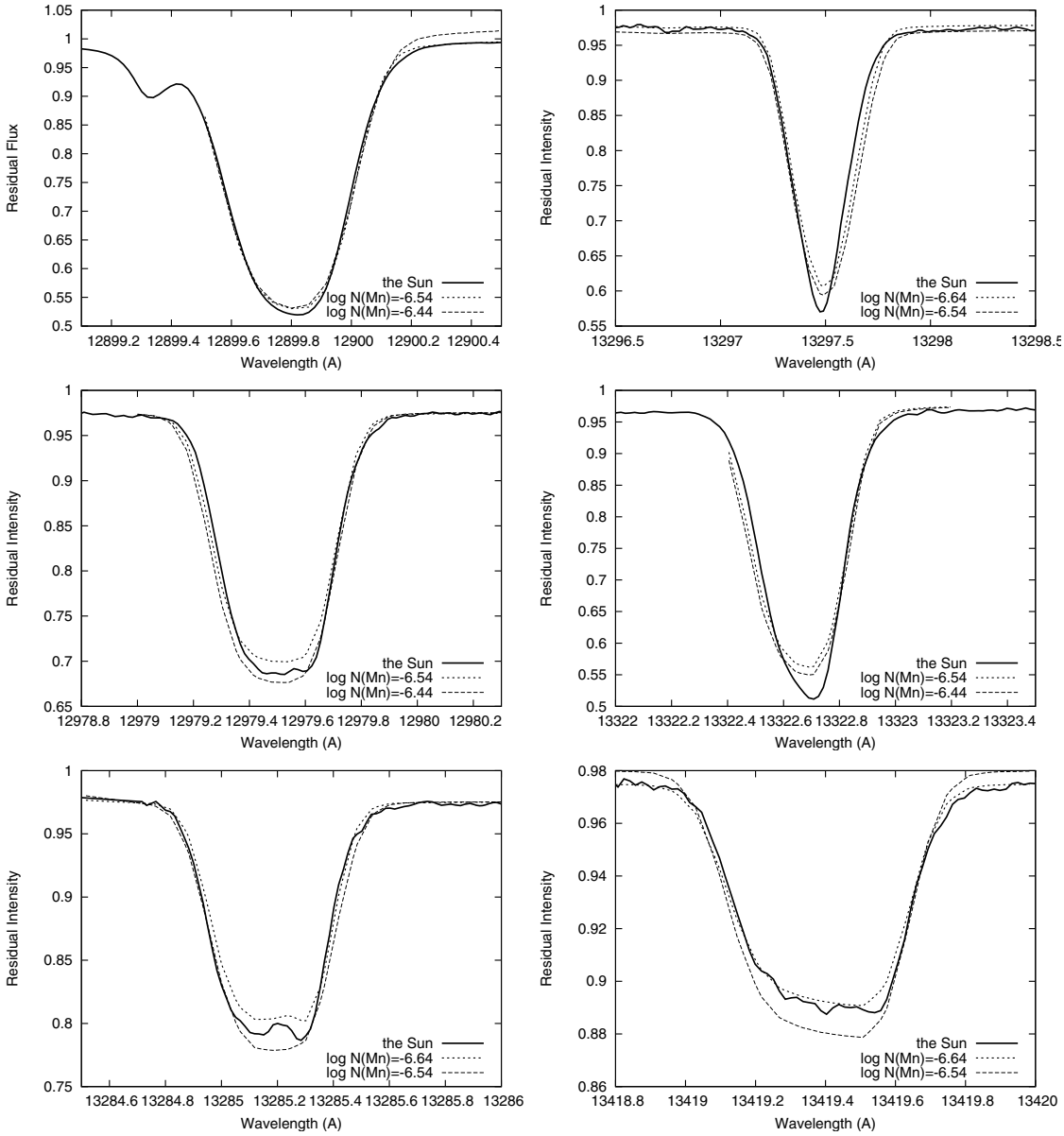

Fig. 3. The best fits to the observed solar spectrum features found from the minima of Eq. (3) for Mn I lines at 12 899 Å, 12 975 Å, 13 281 Å (*left column*) and 13 293 Å, 13 318 Å, 13 415 Å (*right column*). The wavelength scale is taken from the observed spectrum of the Sun.

fitted profiles of the other IR transitions (12 975, 13 281, 13 293, 13 318 and 13 415 Å) are shown in Fig. 3.

4.1. Mn I *lines in spectra of the Sun*

Fits of our synthetic spectra to the observed spectrum of the Sun are shown in Fig. 3. The manganese abundances obtained from the fits are given in Table 3. The $\log N(\mathrm{Mn})$ values in Table 3 are determined from a grid of manganese abundances, using the solar value $\log N(\mathrm{Mn}) = -6.64$ of Gurtovenko & Kostik (1989) and 0.05 and 0.1 dex as the abundance steps for the $\log N(\mathrm{Mn})$ measurements.

Table 3. The Mn I abundances determined from the best fits to the solar spectrum.

Mn I line (approx. Å)	$\log N(\mathrm{Mn})$
12 899	−6.54
12 975	−6.54
13 281	−6.64
13 293	−6.64
13 318	−6.54
13 415	−6.54

Notes. The uncertainty in the $\log N(\mathrm{Mn})$ values is ±0.05 and relates to the step size in the grid of manganese abundances.

4.2. Mn I *lines in spectra of Arcturus*

Manganese lines in the Arcturus spectrum are considerably more blended. Our fits to the observed profiles of Mn I lines are shown in Fig. 4, and the results of manganese abundance determination are shown in Table 4. The increase in the dispersion of the abundance results for Arcturus in comparison to the Sun is predominantly caused by the increase in blended features in the Arcturus spectrum. To minimise the effect of blending we exclude spectral regions with a relatively high number of unidentified blended

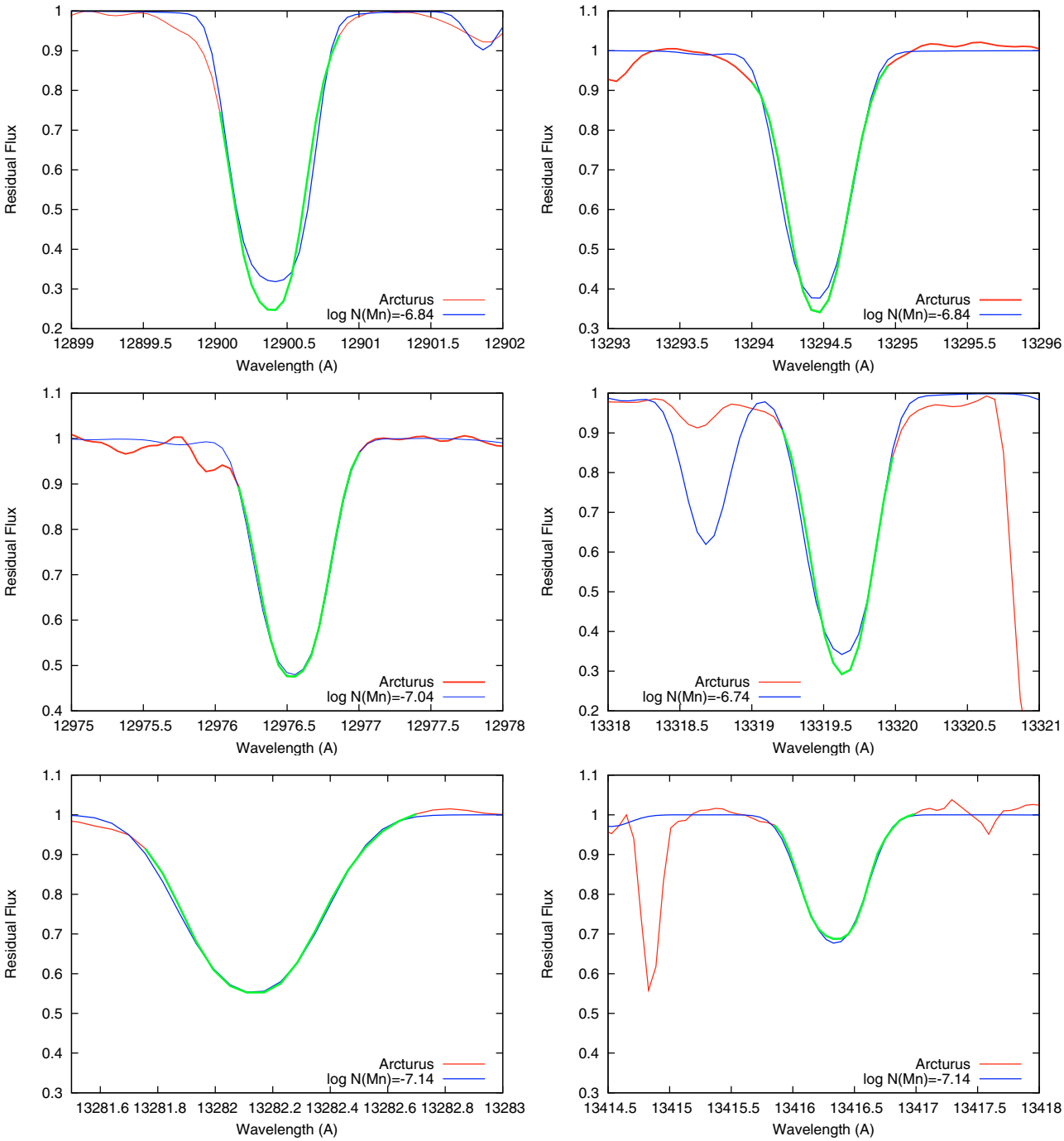

Fig. 4. The best fits to the observed Arcturus spectrum features found from the minima of Eq. (3) for Mn I lines at 12 899 Å, 12 975 Å, 13 281 Å (*left column*) and 13 293 Å, 13 318 Å, 13 415 Å (*right column*). The green line shows the section of the observed profile used to determine manganese abundance. The wavelength scale is taken from the observed spectrum of Arcturus.

Table 4. The Mn I abundances determined from the best fits to the Arcturus spectrum.

Mn I line (fit range, Å)	log N(Mn)
12 899.8–12 900.9	−6.9
12 976.15–12 999.0	−7.1
13 281.7–13 282.7	−7.2
13 294.0–13 295.0	−6.9
13 319.2–13 320.0	−6.8
13 415.8–13 417.0	−7.2

Notes. The uncertainty in the log N(Mn) values is 0.1 and relates to the step size in the grid of manganese abundances.

features when fitting our calculated spectra to the observed spectrum. The corresponding wavelength range for each line is shown in Table 4 and the unblended spectral region used for our fit is marked by a green line in Fig. 4. In addition, in Fig. 5 we provide plots of the dependance of S with log N(Mn) for the Mn I lines (12 899 Å, 12 975 Å, 13 281 Å, 13 293 Å, 13 318 Å, 13 415 Å) observed in the spectrum of Arcturus.

4.3. Mn I *lines in spectra of ultracool dwarfs*

The blending of Mn I lines in the IR spectrum of late-type objects increases significantly for effective temperatures lower than

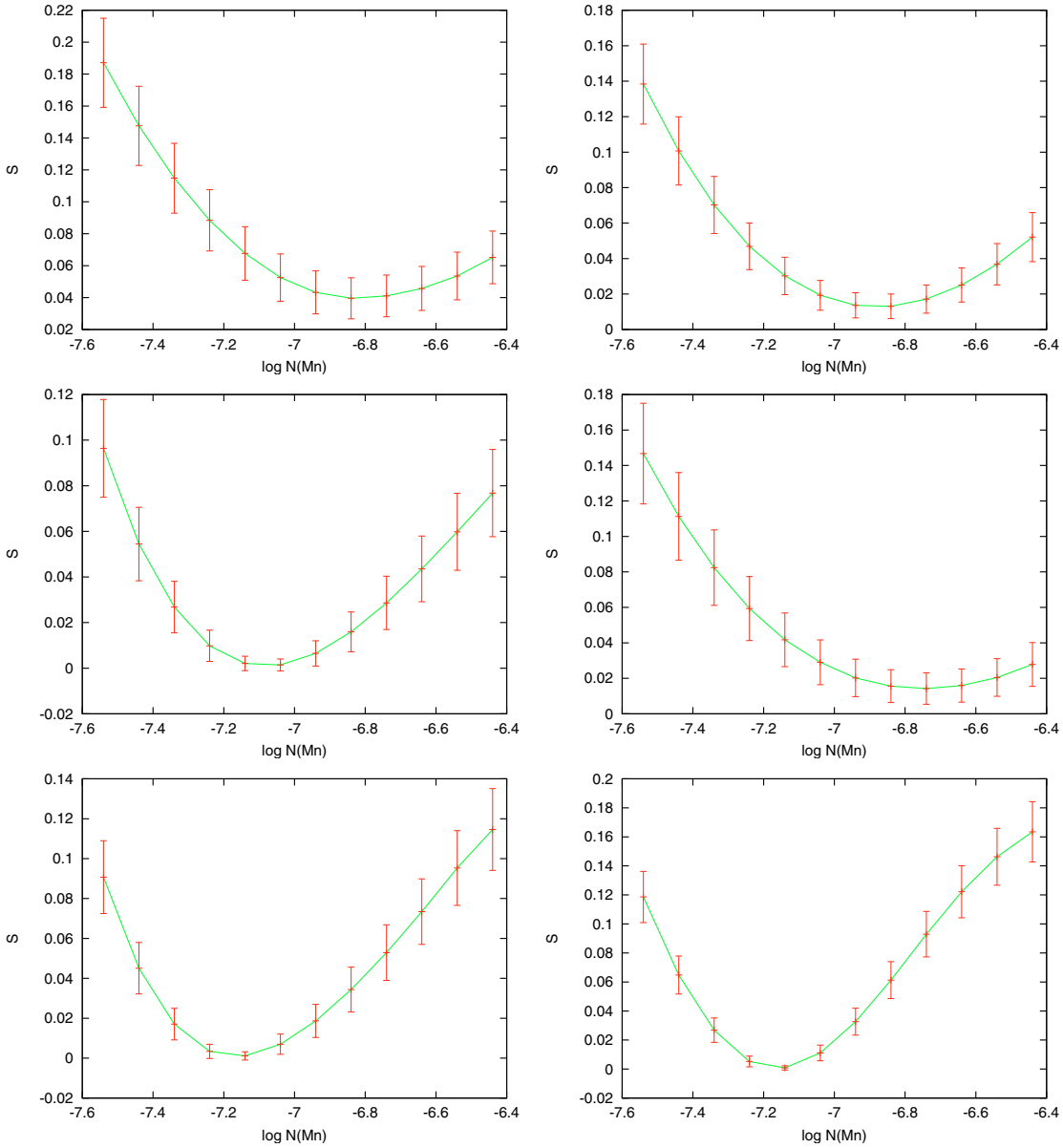

Fig. 5. Dependence of S on $\log N(\mathrm{Mn})$ for the Mn I lines at 12 899 Å, 12 975 Å, 13 281 Å (*left column, top to bottom*) and 13 293 Å, 13 318 Å, 13 415 Å (*right column, top to bottom*) observed in spectrum of Arcturus, see Fig. 4.

3000 K. Numerous water lines form a pseudo background in the spectral region of many of the IR Mn I lines. However, for M9 dwarfs it is possible to fit the observed profiles of some Mn I lines. We provide an example of the profile fit for the Mn I line at 12 899 Å in the spectrum of 2MASSW 0140026+270150. The observed spectrum is described in detail in Lyubchik et al. (2007). The computation was performed with an initial assumption of solar like abundances for manganese, and other elements, and we have determined a value of $\log N(\mathrm{Mn}) = -6.7 \pm 0.2$ in the atmosphere of 2MASSW 0140026+270150, which agrees to within the joint uncertainties with our derived solar abundance for manganese.

Both the line intensity and line profile can be fitted with the solar value of the manganese abundance. However, the spectra of cooler objects are dominated by the water bands in the near-IR, see the computed spectrum of LP944-20 (M 9.5, 2000/4.5 from Pavlenko et al. 2007). For these cooler objects only the Mn I line at 12 899 Å can be used for the analysis because the other lines are too blended with the H_2O bands.

5. Summary

Branching fractions for 20 Mn I transitions have been measured using high resolution Fourier transform spectroscopy and placed on an absolute scale using radiative lifetimes. Fifteen of these transitions have no previously published experimentally measured oscillator strengths. The remaining five transitions agree with previous published oscillator strengths to within the uncertainty of the measurements.

Using our new experimental $\log(gf)$ values we have determined the manganese abundance in the atmosphere of several late type stars. Our solar manganese abundance, $\log N(\mathrm{Mn}) = -6.60 \pm 0.05$, agrees well with the manganese abundances of Anders & Grevesse (1989) $\log N(\mathrm{Mn}) = -6.65$, Gurtovenko & Kostik (1989) $\log N(\mathrm{Mn}) = -6.64$, and Biemont (1975) $\log N(\mathrm{Mn}) = 6.67$. Blending affects Mn I lines in the IR spectra of stars cooler than the Sun. As a result, our manganese abundances obtained from the fits to different lines in the spectrum of Arcturus are in the range $-6.75 < \log N(\mathrm{Mn}) < -7.15$, with a

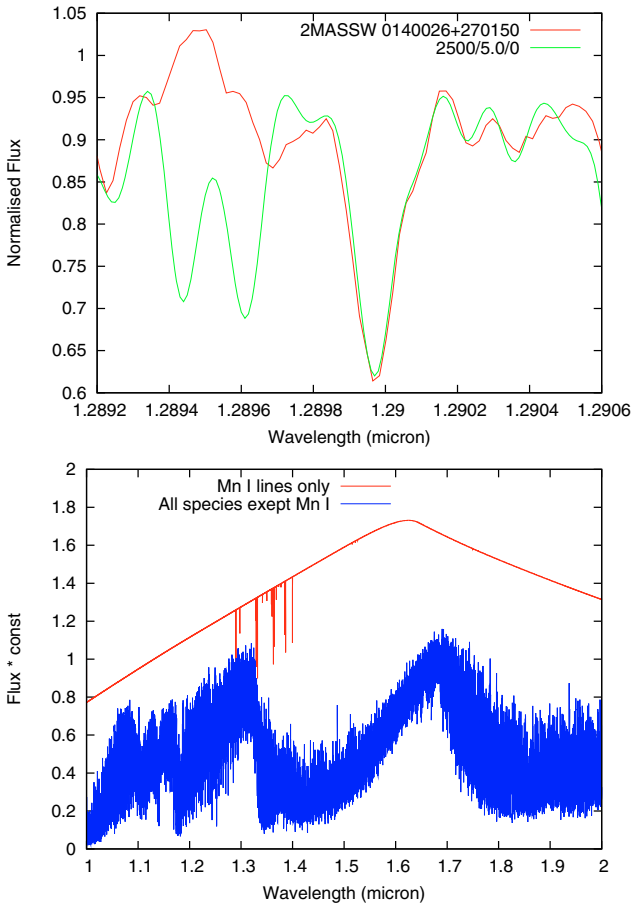

Fig. 6. *Top*: the manganese line at 12 899 Å in the spectrum of M 9.5 dwarf 2MASSW 0140026+270150, where the red line is the observed spectrum and the green line is the model spectrum using our oscillator strengths and hyperfine component line positions ($T_{\rm eff}$/ log(g)/[Fe/H] = 2500/5.0/0.0). *Bottom*: a comparison of the calculated spectrum of LP944-20 with only absorption features from Mn I in red and all other atomic and molecular species including the water vapour bands in blue.

mean log N(Mn) = −6.95 ± 0.20, which agrees to within the uncertainty with the log N(Mn) = −6.97 determined by McWilliam et al. (2003) for Arcturus. Furthermore, our new laboratory measured log(gf)s for IR Mn I spectral lines can be used in the study of dust obscured objects and as a secondary abundance check to abundance studies using Mn I spectral lines in the visible.

Acknowledgements. We thank Drs. L. Prato and I. S. McLean for providing the 2MASSW 0140026+270150 spectrum. R.B.W. gratefully acknowledges the European Commission for a Marie Curie fellowship. J.C.P., Y.P. and H.R.A.J. gratefully acknowledge funding from the Leverhulme Trust and STFC, UK. The work of Y.P. and L.Y. was partially supported by the Microcosmophysics-2 program of the National Academy and Space Agency of Ukraine. H.N. acknowledges the support of the Linnaeus grant to the Lund Laser Centre from the Swedish Research Council.

References

Allard, F., Hauschildt, P. H., Alexander, D. R., Tamanai, A., & Schweitzer, A. 2001, ApJ, 556, 357
Anders, E., & Grevesse, N. 1989, Geochim Cosmochim. Acta, 53, 197
Barber, R. J., Tennyson, J., Harris, G. J., & Tolchenov, R. 2006, MNRAS, 368, 1087
Biemont, E. 1975, Sol. Phys., 44, 269
Bigot, L., & Thévenin, F. 2006, MNRAS, 372, 609
Birch, K. P., & Downs, M. J. 1994, Metrologia, 31, 315
Blackwell-Whitehead, R. J., Xu, H. L., Pickering, J. C., Nave, G., & Lundberg, H. 2005a, MNRAS, 361, 1281
Blackwell-Whitehead, R. J., Pickering, J. C., Pearse, O., & Nave, G. 2005b, ApJS, 157, 402
Blackwell-Whitehead, R. J., Pickering, J. C., Jones, H. R. A., et al. 2008, J. Phys.: Conf. Ser., 130, 012002
Bond, J. C., Lauretta, D. S., Tinney, C. G., et al. 2008, ApJ, 682, 1234
Booth, A. J., Blackwell, D. E., Petford, A. D., & Shallis, M. J. 1984, MNRAS, 208, 147
Brickhouse, N., Federman, S., Kwong, V., et al. 2006, Laboratory Astrophysics White Paper, Proceedings of the NASA Lab. Astro. Workshop, http://adsabs.harvard.edu/abs/2006nla..conf....1B
Brodzinski, T., Kronfeldt, H. D., Kropp, J. R., & Winkler, R. 1987, Z. Phys. D, 7, 161
Burrows, A., Ram, R. S., Bernath, P., Sharp, C. M., & Milson, J. A. 2002, ApJ, 577, 986
Catalán, M. A., Meggers, W. F., & Garcia-Riquelme, O. 1964, J. Res. Natl. Bur. Stand., 68A, 9
Dembczyński, J., Ertmer, W., Johann, U., Penselin, S., & Stinner, P. 1979, Z. Phys. A, 291, 207
Dulick, M., Bauschlicher, C. W., Jr., Burrows, A., et al. 2003, ApJ, 594, 651
Edlén, B. 1966, Metrologia, 2, 71
Fuhr, J. R., & Wiese W. L. 2003, NIST Atomic Transition Probability Tables, in Handbook of Chemistry and Physics, 84th edition, ed. D. R. Lide (Boca Raton, FL: CRC Press), 10, 93
Gray, D. F. 1976, The observation and analysis of stellar photospheres (New York: Wiley-Interscience), 484
Gurtovenko, E. A., & Kostyk, R. I. 1989, Fraungoferov spektr i sistema solnechnykh sil ostsilliatorov (Kiev: Nauk. Dumka)
Handrich, E., Steudel, A., & Walther, H. 1969, Phys. Lett., 29A, 486
Hinkle, K., Wallace, L., & Livingston, W. 1995, PASP, 107, 1402
Johansson, S. 2005, Atomic Data in the 1–5 Micron Region: Present Status in High Resolution Infrared Spectroscopy in Astronomy (Berlin: Springer), 62
Jones, H. R. A., Pavlenko, Y. V., Tennyson, J., & Viti, S. 2002, MNRAS, 330, 675
Jones, H. R. A., Viti S., Tennyson, J., et al. 2005, Astron. Nachr., 326, 920
Kronfeldt, H. D., Kropp, J. R., Subaric, A., & Winkler, R. 1985, Z. Phys., 322, 349
Kuhn, H. G. 1964, Atomic Spectra (London: Longmans), 329
Kupka, F., Piskunov, N. E., Ryabchikova, T. A., Stempels, H. C., & Weiss, W. W. 1999, A&AS 138, 119
Kurucz, R. L. 1991, The solar spectrum, Solar interior and atmosphere (A92–36201 14-92) (Tucson, AZ: University of Arizona Press), 663
Kurucz, R.l. 1993, A new opacity-sampling model atmosphere program for arbitary abundances, Peculiar versus normal phenomena in A-type and related stars, ed. M. M. Dworetsky, F. Castelli, & R. Faragianna, ASP Conf. Ser., 44, 87
Kurucz, R. L., & Bell, B. 1995, Atomic Line Data, Kurucz CD-ROM No. 23., Cambridge, Mass.: Smithsonian Astrophysical Observatory
Lyubchik, Y., Jones, H. R. A., Pavlenko, Y. V., et al. 2004, A&A, 416, 655
Lyubchik, Y., Jones, H. R. A., Pavlenko, Y. V., et al. 2007, A&A, 473, 257
Meléndez, J. 1999, MNRAS, 307, 197
Nave, G., Sansonetti, C. J., & Griesmann, U. 1997, in Opt. Soc. Am. Tech. Digest Series, 3, Fourier transform spectroscopy: Methods and Applications (Washington DC: Opt. Soc. Am.), 38
McWilliam, A., Rich, R. M., & Smecker-Hane, T. A. 2003, ApJ, 592, 21
Pavlenko, Ya. V. 2000, Astron. Rep., 44, 219.
Pavlenko, Ya. V. 2003, Astron. Rep., 47, 59
Pavlenko, Ya. V., & Jones, H. R. A. 2002, A&A, 396, 967
Pavlenko, Ya. V., Jones, H. R. A., Martín, E. L., et al. 2007, MNRAS, 380, 1285
Peterson, R., Ore, C. M. D., & Kurucz, R. 1993, ApJ, 404, 333
Pickering J. C. 2002, Vib. Spectrosc., 29, 27
Plez, B. 1998, A&A, 337, 495
Prochaska, J. X., & McWilliam, A. 2000, ApJ, 537, L37
Ralchenko, Yu., Kramida, A. E., Reader, J., & NIST ASD Team 2008, NIST Atomic Spectra Database (version 3.1.5), http://physics.nist.gov/asd3 [2009, June 18], National Institute of Standards and Technology, Gaithersburg, MD
Schnabel, R., Bard, A., & Kock, M. 1995, Z. Phys. D, 34, 223
Sikström, C. M., Nilsson, H., Litzén, U., Blom, A., & Lundberg, H. 2002, J. Quant. Spec. Rad. Trans., 74, 355
Sobeck, J. S., Ivans, I. I., Simmerer, J. A., et al. 2006, AJ, 131, 2949
Taylor, B. N., & Kuyatt, C. E. 1994, Guidelines for Evaluating and Expressing the Uncertainty of NIST Measurement Results, NIST Technical Note, 1297
Unsöld, A. 1955, Physik der Sternatmospheren, 2nd edn. (Berlin: Springer)
Wahlgren, G. M., & Johansson, S. 2003, GAIA Spectroscopy: Science and Technology, ASP Conf. Proc., ed. U. Munari, 298, 481